Dynamic behavior of postfilamentation Raman pulses

Jean-François Daigle,[1,*] Tie-Jun Wang,[1] Sima Hosseini,[1] Shuai Yuan,[1] Gilles Roy,[2] and See Leang Chin[1]

[1]Centre d'Optique, Photonique et Laser (COPL) et Département de physique, de génie physique et d'optique, Université Laval, Québec, Québec G1V 0A6, Canada

[2]Defence Research and Development Canada-Valcartier, Québec, Québec G3J 1X5, Canada

*Corresponding author: jfdaigle2@yahoo.ca

Received 2 June 2011; accepted 8 August 2011;
posted 21 September 2011 (Doc. ID 148539); published 16 November 2011

We report on the postfilamentation behavior of a Stokes pulse created from intense and collimated ultrashort pulses propagating in air. A systematic analysis of the pulse propagation revealed that the redshifted Raman pulse produced during filamentation had a larger divergence than the postfilamentation intense pump pulse. Also, the analysis of the far-field Stokes transverse ring revealed that the intensity in this ionization-free light channel is still sufficiently high to induce stimulated Raman scattering after ionization had ended. This behavior further extends the potential of filamentation to remotely induce third-order nonlinearities. © 2011 Optical Society of America

OCIS codes: 010.1300, 260.5950, 190.5940.

1. Introduction

Filamentation [1–6] of ultrashort pulses in air results from a dynamic interplay between two opposing nonlinear contributions: self-focusing attributed to the intensity-dependent refractive index and defocusing induced by the self-generated plasma. In air, filaments produced from collimated pulses whose power is larger than the critical power [7] can extend over hundreds of meters [8] and, for laser pulses centered at 800 nm, maintain a clamped intensity [9,10] that is about 5×10^{13} W/cm^2. Depending on the initial pulse conditions, after the intensity had dropped below the ionization threshold ($\sim 10^{13}$ W/cm^2), an intense, low divergence light channel was observed for even longer distances [11,12].

Similar to optical fibers, filaments are self-induced structures where light can be confined at extremely high intensities over extended distances. These are ideal conditions for efficient nonlinear energy conversion and, at filament-level intensities, air becomes a highly active nonlinear medium. For example, during filamentation, laser pulses undergo spectral modifications induced by self-phase modulation, four-wave mixing [13,14], and stimulated Raman scattering (SRS) [15,16]. Even though the first two effects are related to the anharmonic response of the bound electrons while SRS involves the excitation of molecular rotational states (mainly N_2 and O_2 in air), these are all nonlinear intensity-dependent mechanisms. As a consequence, nonlinear self-focusing can enhance the Raman process by increasing the on-axis intensity.

The spectral modifications induced by SRS are characterized by the scattering of laser energy at the fundamental frequency into multiple Stokes and anti-Stokes frequencies. This mechanism is described by a three-level nonresonant molecular process between a nonpopulated higher energy virtual state and two lower energy rotational/vibrational states. Under the impulsive excitation of the laser, the molecules are almost instantaneously aligned and start to rotate at a speed that depends on the torque applied on the individual molecules. As a result, delayed molecular alignments are observed [17]. For femtosecond pulses, only the initial molecular alignment has a contribution because the second alignment time (quarter revival) occurs for N_2 approximately 2.1 ps after the pulse excitation. In air,

0003-6935/11/336234-05$15.00/0

the characteristic instantaneous full alignment time is approximately 80 fs. Because of the dispersive properties of air, SRS emissions can propagate at large angles with respect to the propagation axis. In a Raman-active liquid, those large angle emissions allowed the observation of an X-wave pattern in the Stokes' angular-spectral distribution [18].

For very long pulse durations (>10 ps), the transient effects linked to the delayed response are negligible and the Raman gain is mainly governed by the intensity of the pump pulse. However, as the pulse duration is decreased, the Raman gain continuously grows due to the pulse's increasing spectral width, which excites larger and larger molecular rotational states. As a result, long pulses induce narrow spectral lines centered at the Stokes and anti-Stokes frequencies, while short and spectrally broad pulses produce a "quasi-continuum" of Raman frequencies [16]. This enhancement continues until the laser pulse becomes shorter than the rotational period (<2.1 ps in air) of the molecules where a drastic decrease of the Raman gain is observed [15].

Even though the Raman gain should be very weak, strong SRS amplification of Stokes frequencies has been observed for femtosecond pulses during filamentation in air [19]. In fact, even if the Raman contribution is small, the high intensity inside the filament core and the long interaction length provide good conditions for near-axis amplification of a Stokes pulse with an excellent beam quality. In addition, cascaded self-frequency downshifting of a laser pulse was attributed to SRS during filamentation in air [20].

This work is a direct continuation of the results reported in Refs. [12,20]. Indeed, we report on the postfilamentation behavior of a Raman Stokes pulse created from inside the intense and collimated ultrashort filamenting pulse propagating in air. A systematic analysis of the pulse propagation performed after the end of the filament revealed that the intensity in this ionization-free channel is still sufficiently high to induce SRS long after the filament had ended. The Raman pulse was mainly redshifted with respect to the fundamental beam and had a larger divergence than the postfilamentation intense pump pulse. This result indicates that even though the postfilament beam cannot ionize air, its intensity can still induce appreciable third-order nonlinearities, such as Kerr self-focusing (Refs. [11,12]) and, in this case, SRS. This result further extends the potential of laser filamentation to be used as a remote, broadband atmospheric lamp [21].

2. Experimental Methods and Results

Collimated transform limited laser pulses (5 mJ/45 fs), emitted at a 10 Hz repetition rate from a typical Ti:sapphire amplifier, were launched in a 25 m long corridor. The laser pulses were initially elliptical in shape and characterized with 3.6 mm and 2.5 mm transverse diameters at full width at half-maximum (FWHM). The initial pulse conditions ensured that a stable single filament occurred at almost every laser shot. The evolution of the laser pulses was characterized along the propagation axis using a mobile experimental unit.

The experimental unit is presented in Fig. 1. First of all, the number of free electrons produced along the filament was characterized by measuring the intensity of the N_2 fluorescence with a photomultiplier tube (PMT) together with a UG11 filter. For each position, the N_2 fluorescence was imaged, with a one-to-one magnification, onto the surface of the PMT such that a 5 mm long section of the filament limited by the diameter of the sensitive surface was detected. The spectra were measured using an ocean optic fiber spectrometer coupled to an integration sphere. A 2.0 mm diameter iris ensured that mainly the intense filament/postfilament core went into the sphere. We call these the on-axis spectra. In order to limit the nonlinearities on the solid surfaces and avoid damaging the material, only a weak reflection from the front surface of a bulk fused silica wedge was used to perform the measurement. Finally, the beam patterns were measured with a CCD camera using bandpass filters centered at 800 nm (BP800) and 850 nm (BP850) to observe either the behavior of the pulse's fundamental wave or that of the Stokes-shifted frequencies. BP800 and BP850 each had a 10 nm transmission bandwidth. In this case, the wedge's front surface reflection was incident onto a spectrally flat white diffuser. The CCD camera

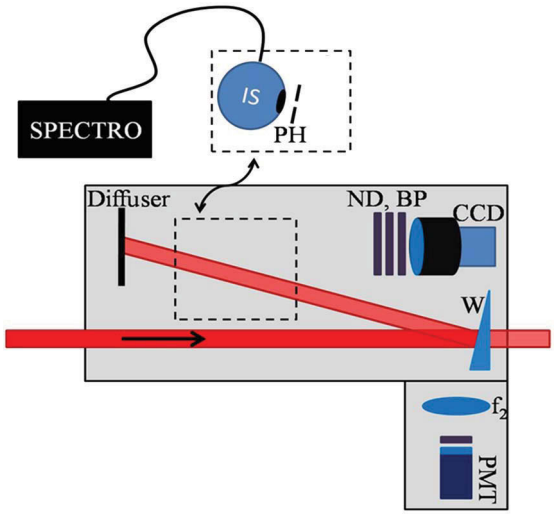

Fig. 1. (Color online) Experimental unit that was moved along the beam. At each position, three measurements were performed. The weak reflection from a bulk fused silica wedge is directed to an integration sphere (IS) connected to a fiber spectrometer. A 2.0 mm diameter iris (PH) was inserted before IS to measure the filament/hot spot spectrum. IS and PH were then removed and W's front surface reflection was directed to a spectrally flat diffuser. A CCD camera imaged the scattered beam pattern for various spectral windows (bandpass filters, BP). Finally, the wedge was removed and N_2 fluorescence was imaged onto the sensitive surface of a photomultiplier tube (PMT) with a fused silica lens ($f_2 = 6$ cm). A UG11 filter and a 800 nm dielectric mirror ensured that the detected signal was attributed to N_2 fluorescence.

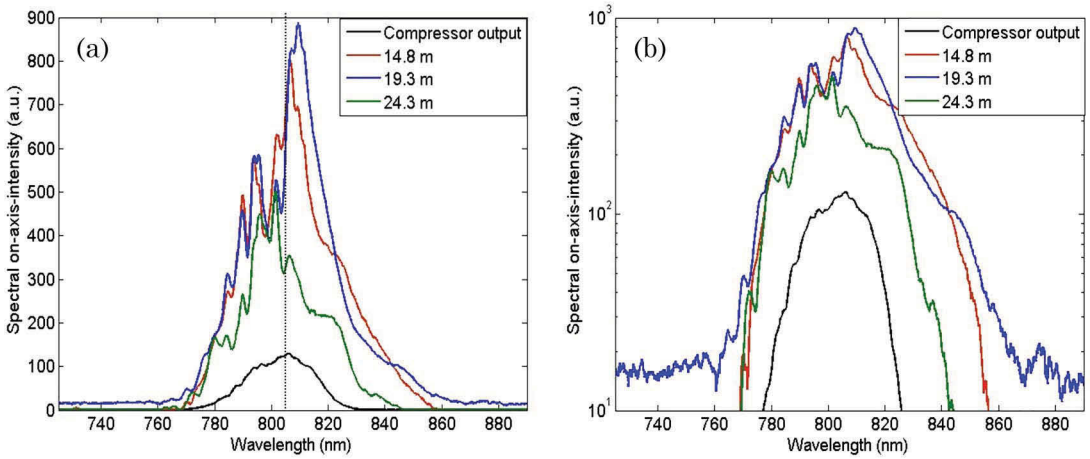

Fig. 2. (Color online) On-axis spectra measured using a fiber spectrometer coupled to an integration sphere. A 2.5 mm diameter pinhole ensured that only the filament/postfilament hot spot entered the sphere. Spectra are presented for different positions in (a) linear and (b) logarithmic scales.

measured the scattered patterns of the pulses; appropriate neutral density (ND) filters were used to avoid saturation of the detector. These measurements were performed at every 50 cm along the 25 m propagation length.

In order to discriminate the shifted Stokes frequencies, let us first take a look at Fig. 2, which shows the on-axis spectra, in linear (a) and logarithmic (b) scales. The propagation starts at the compressor's output (black) with the spectrum centered at $\lambda_0 = 803$ nm with a 22 nm spectral width at FWHM. As mentioned earlier, the Raman effect can scatter shifted photons at large angles with respect to the propagation axis. However, with femtosecond pulses during filamentation, mainly axial or near axial scattered photons can be amplified via SRS such that the effect of their divergence can only be observed near the beam axis in the far field [16]. This is why the selected spectra were measured after the filament had ended. To learn more about the spectral evolution of femtosecond laser pulses during filamentation in air, please refer to Refs. [1,16,19,20].

Near the end of the filament (14.8 m from the compressor, red), the on-axis spectra exhibited a moderate amplification accompanied by strong modulations on the blue side of λ_0. The modulations indicate that this type of spectral broadening was mainly attributed to the interaction of the pulse's trailing edge with the plasma formed at the peak of the pulse. On the other hand, the spectral intensity for wavelengths larger than λ_0 presented strong axial enhancement with almost no modulations. This on-axis intensity enhancement is the consequence of self-focusing of the laser pulse while the spectral broadening toward longer wavelengths is dominantly attributed to SRS. When we look at that spectrum, we can immediately draw a line [dotted, Fig. 2(a)] between the two regimes and this limit is positioned at exactly λ_0. This is a direct consequence of group-velocity dispersion in air where the longer wavelengths propagate faster. Therefore, the shorter wavelengths diffract/refract on the plasma behind the leading edge. Interestingly, from 14.8 to 19.3 m (blue), the on-axis spectrum continues to evolve toward longer wavelengths even if the filament had ended almost 5 m before. Meanwhile, the $\lambda < \lambda_0$ spectral region remained almost constant. This suggests that SRS could still play an important role during postfilamentation propagation.

However, between 19.3 and 24.3 m (green), the spectral intensity for $\lambda > \lambda_0$ suffered a drastic depletion. As it will be discussed in the following paragraphs, this drastic signal depletion was caused by the emission of the transverse ring and the larger divergence of the Raman pulse. However, the axial intensity is still much higher than what it used to be at the compressor's output.

This is clearly shown in Fig. 3, which presents beam patterns measured along the propagation axis. The top row corresponds to pictures captured using BP800 and the bottom row, BP850. The latter filter was selected to observe the behavior of the Stokes frequencies with limited contamination from the fundamental pulse. We should emphasize that other Stokes frequencies could have different characteristics (emission angle, energy), this spectral range around 850 nm is only used to show the overall behavior of the SRS pulse. For each picture, the distance from the compressor and the transmission of the combined ND and BP filters are indicated on the top left corner.

The pictures measured at 800 nm are almost identical to those presented in Ref. [12] because similar laser pulses (same laser, same conditions, different days) were used. They show the evolution of the pulse from the beginning of filamentation (8.8 m) to the postfilamentation ionization-free regime (> 15 m). On the other hand, the Stoke-shifted pulse presented a beam profile of excellent quality attributed to the self-cleaning process [19] that occurred during filamentation. However, the far-field divergence of the hot spot at 850 nm was significantly

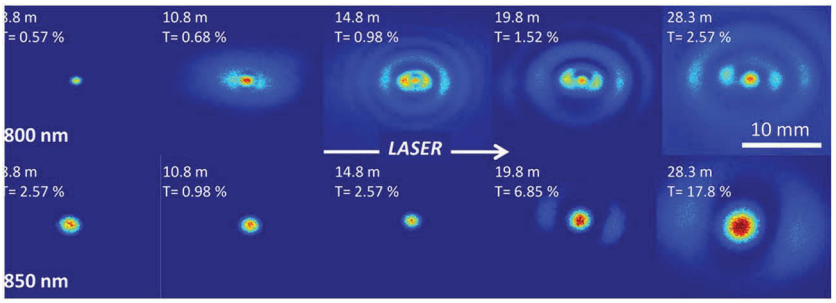

Fig. 3. (Color online) Beam patterns measured along the propagation direction using a CCD camera protected with bandpass filters centered at 800 nm (top row) and 850 nm (bottom row).

larger such that the core diameter was already 2.6 mm FWHM at 28.3 m (compared to 1.6 mm for 800 nm). Because of the increasing filter transmission, a concentric ring could be observed starting from 18 m when using BP850. The formation of this ring is partly responsible of the Stokes-shifted frequencies' axial depletion observed in Fig. 2. As we will see, the effects of linear dispersion on SRS are responsible for its formation [15] and this subject will be discussed in the following section.

The hot spot diameter, measured from the pictures taken using BP800 (black circles) and BP850 (blue squares), is plotted as a function of distance in Fig. 4. As an indication, the molecular N_2 fluorescence intensity (red triangles) is also plotted as a function of distance showing a filament staring at 9.5 m and ending near 14.5 m. This figure reveals that the divergence of the Raman pulse is 0.15 ± 0.1 mrad, while that of the postfilament ionization-free channel is 0.03 ± 0.1 mrad. This explains the spectral depletion of the Stokes wavelengths observed in Fig. 1 beyond 20 m.

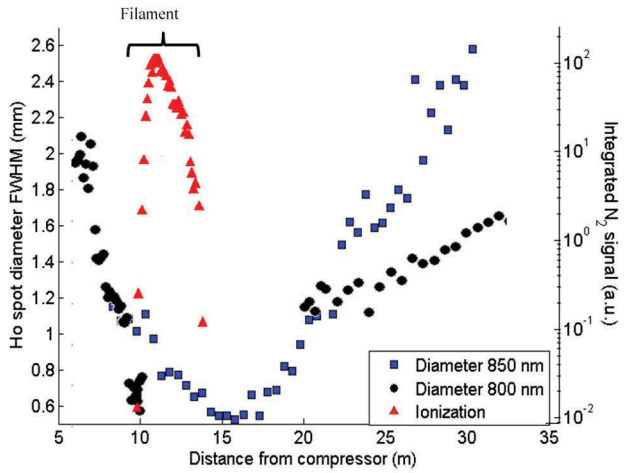

Fig. 4. (Color online) Hot spot diameters FWHM plotted as a function of the distance from the compressor. The black circles show the data measured using BP800 and the blue squares, the data obtained with BP850. The red triangles correspond to the fluorescence signal intensity measured along the beam with a PMT. The corresponding scale is on the right-hand side of the figure.

3. Postfilamentation SRS

It is now clear that a laser filament formed from femtosecond pulses can produce a Stokes pulse via SRS [19,20]. However, to the best of our knowledge, there is no evidence as to, whether or not, the postfilament light channels can induce SRS. The divergence angle of the concentric ring observed using BP850, in Fig. 3, provides information related to the laser intensity required to produce that ring.

As reported by Peñano *et al.* [15], the scattered angle of the Stokes pulse via SRS from intense laser pulses can be described by the following approximate, analytical expression, which relates the angle of perfect phase matching θ_0 to the pump laser intensity I_0:

$$\cos\theta_0 \approx 1 - \frac{\beta_2(\omega_R^2 + \Gamma_2^2)}{2k_0} - \frac{(n_K + n_R)}{n_0}\left(\frac{\omega_R^2 + \Gamma_2^2}{\omega_0^2}\right) I_0.$$

θ_0 corresponds to the angle where two pump, one Stokes, and one anti-Stokes photons are totally phased matched [18]. This angular region is characterized by a zero Raman gain, i.e., it is located somewhere in the solid angle located between the ring and the central spot. In this relation, k_0 is the wave vector, n_0 is the medium's linear index of refraction, ω_0 is the angular frequency, β_2 is the group-velocity dispersion parameter, ω_R is the molecular rotational frequency, and Γ_2 is the dipole dephasing rate. n_K and n_R are the nonlinear contributions to the index of refraction attributed to the Kerr and rotational Raman effects, respectively. Because of Raman's delayed response, in the short pulse limit, $n_R \to 0$.

In air, with 800 nm laser pulses, we have $\beta_2 = 2.2 \times 10^{-31}\,\mathrm{s^2/cm}$, $\Gamma_2 = 1.3 \times 10^{13}\,\mathrm{s^{-1}}$, $\omega_R = 16 \times 10^{12}\,\mathrm{s^{-1}}$, and $n_K = 3 \times 10^{-19}\,\mathrm{cm^2/W}$ [16]. Now assuming that this ring was formed in the intense filament core, where we would expect an intensity neighboring $I_0 = 5 \times 10^{13}\,\mathrm{W/cm^2}$, the perfect phase matching angle would be $\theta_0 = 4.88$. However, based on our measurement, this angle is approximately $\theta_0 = 0.27 \pm 0.02$ mrad such that the high intensity inside the filament core could not be responsible for this ring. The Raman ring emitted at those large angles during filamentation was not detected due to the strong attenuation provided by the neutral density filters located in front of the CCD.

An angle θ_0 comparable to the measured data can be obtained with laser intensities $I_0 \approx 2 \times 10^{11}\,\mathrm{W/cm^2}$, which gives $\theta_0 = 0.29\,\mathrm{mrad}$. This is not too far from the intensity of the postfilamentation ionization-free channels measured in Refs. [11,12]. This result would imply that the intensity inside those channels is sufficiently high to induce SRS and amplifies Stokes frequencies. Indeed, assuming a linear divergence of this ring (it is linear based on our observation), its origin can be traced back to 15–17 m after the compressor, 2 m after ionization had ended. Based on the results presented in Fig. 2, this type of postfilamentation SRS amplification still occurred ~5 m after the filament ended.

4. Conclusion

In this paper, we reported on the postfilamentation dynamics of a redshifted Raman pulse produced via SRS. This Stokes pulse presented an excellent beam profile, attributed to the self-cleaning process occurring during filamentation. Because SRS can amplify photons that propagate at large angles with respect to the propagation axis, the Raman pulse diverged almost 4 times faster than the postfilament intense light channel. This behavior was observed in both the measured on-axis spectra and the beam patterns measured at 850 nm.

Furthermore, an analysis of the transverse Raman ring divergence revealed that the intensity in the postfilament light channels is sufficiently high to further amplify a Stokes pulse via SRS. This newly discovered property extends the potential of filamentation nonlinear optics [22] to produce broadband laser pulses. Indeed, intense postfilamentation channels were observed km after the laser source, thus providing a very long nonlinear interaction zone.

We acknowledge the support from the Natural Sciences and Engineering Research Council, Defense Research and Development in Canada–Valcartier, the Canadian Institute for Photonic Innovation, the Canadian Foundation for Innovation, Fonds Québécois de Recherche pour la Nature et la Technologie, and the Canadian Research Chair. We would also like to thank Dr. Francis Théberge for fruitful discussions.

References

1. A. Couairon and A. Mysyrowicz, "Femtosecond filamentation in transparent media," Phys. Rep. **441**, 47–189 (2007).
2. L. Bergé, S. Skupin, R. Nuter, J. Kasparian, and J.-P. Wolf, "Ultrashort filaments of light in weakly ionized, optically transparent media," Rep. Prog. Phys. **70**, 1633–1713 (2007).
3. V. P. Kandidov, S. A. Shlenov, and O. G. Kosareva, "Filamentation of high-power femtosecond laser radiation," Quantum Electron. **39**, 205–228 (2009).
4. S. L. Chin, S. A. Hosseini, W. Liu, Q. Luo, F. Théberge, N. Aközbek, A. Becker, V. P. Kandidov, O. G. Kosareva, and H. Schroeder, "The propagation of powerful femtosecond laser pulses in optical media: physics, applications, and new challenges," Can. J. Phys. **83**, 863–905 (2005).
5. J. Kasparian and J.-P. Wolf, "Physics and applications of atmospheric nonlinear optics and filamentation," Opt. Express **16**, 466–493 (2008).
6. S. L. Chin, *Femtosecond Laser Filamentation* (Springer-Verlag, 2010).
7. W. Liu and S. L. Chin, "Direct measurement of the critical power of femtosecond Ti:sapphire laser pulse in air," Opt. Express **13**, 5750–5755 (2005).
8. G. Méchain, C. D'Amico, Y.-B. André, S. Tzortzakis, M. Franco, B. Prade, A. Mysyrowicz, A. Couairon, E. Salmon, and R. Sauerbrey, "Range of plasma filaments created in air by a multi-terawatt femtosecond laser," Opt. Commun. **247**, 171–180 (2005).
9. J. Kasparian, R. Sauerbrey, and S. L. Chin, "The critical laser intensity of self-guided light filaments in air," Appl. Phys. B **71**, 877–879 (2000).
10. A. Becker, N. Akozbek, K. Vijayalakshmi, E. Oral, C. M. Bowden, and S. L. Chin, "Intensity clamping and re-focusing of intense femtosecond laser pulses in nitrogen molecular gas," Appl. Phys. B **73**, 287–290 (2001).
11. G. Méchain, A. Couairon, Y.-B. André, C. D'Amico, M. Franco, B. Prade, S. Tzortzakis, A. Mysyrowicz, and R. Sauerbrey, "Long-range self-channeling of infrared laser pulses in air: a new propagation regime without ionization," Appl. Phys. B **79**, 379–382 (2004).
12. J.-F. Daigle, O. Kosareva, N. Panov, T.-J. Wang, S. Hosseini, S. Yuan, G. Roy, and S. L. Chin, "Formation and evolution of intense, post-filamentation, ionization-free low divergence beams," Opt. Commun. **284**, 3601–3606 (2011).
13. F. Théberge, N. Aközbek, W. Liu, A. Becker, and S. L. Chin, "Tunable ultrashort laser pulses generated through filamentation in gases," Phys. Rev. Lett. **97**, 023904 (2006).
14. D. J. Cook and R. M. Hochstrasser, "Intense terahertz pulses by four-wave rectification in air," Opt. Lett. **25**, 1210–1212 (2000).
15. J. R. Peñano, P. Sprangle, P. Serafim, B. Hafizi, and A. Ting, "Stimulated Raman scattering of intense laser pulses in air," Phys. Rev. E **68**, 056502 (2000).
16. J. R. Peñano, P. Sprangle, B. Hafizi, A. Ting, D. F. Gordon, and C. A. Kapetanakos, "Propagation of ultra-short, intense laser pulses in air," Phys. Plasmas **11**, 2865–2874 (2004).
17. A. M. Zheltikov, "Raman response function of atmospheric air," Opt. Lett. **32**, 2052–2054 (2007).
18. D. Faccio, A. Dubietis, G. Tamosauskas, P. Polesana, G. Valiulis, A. Piskarskas, A. Lotti, A. Couairon, and P. Di Trapani, "Phase- and group-matched nonlinear interactions mediated by multiple filamentation in Kerr media," Phys. Rev. A **76**, 055802 (2007).
19. W. Liu and S. L. Chin, "Abnormal wavelength dependence of the self-cleaning phenomenon during femtosecond-laser-pulse filamentation," Phys. Rev. A **76**, 013826 (2007).
20. Y. Chen, F. Théberge, C. Marceau, H. Xu, N. Aközbek, O. Kosareva, and S. L. Chin, "Observation of filamentation-induced continuous self-frequency down shift in air," Appl. Phys. B **91**, 219–222 (2008).
21. L. Wöste, C. Wedekind, H. Wille, P. Rairoux, B. Stein, S. Nikolov, C. Werner, S. Niedermeier, F. Ronneberger, H. Schillinger, and R. Sauerbrey, "Femtosecond atmospheric lamp," Laser Und Optoelektronik **29**, 51–53 (1997).
22. S. L. Chin, F. Théberge, and W. Liu, "Filamentation nonlinear optics," Appl. Phys. B **86**, 477–483 (2006).